

13A.7 A WIND TUNNEL STUDY OF STABLY STRATIFIED FLOW ON A RIDGE COVERED WITH A TALL PLANT CANOPY

John J. Finnigan and Dale Hughes
CSIRO Marine and Atmospheric Research, Canberra, Australia

1. INTRODUCTION

A large fraction of the 450+ Flux Tower sites that comprise the FLUXNET (Baldocchi et al, 2001) suffer from advective flows at night, which are now known to be caused by gravity currents (eg. Staebler and Fitzjarrald, 2005). These flows severely compromise the ability of these towers to compute 24 hour carbon budgets as the advective component of the respiration flux cannot be measured from a single tower. Devising robust correction methods depends on reaching a much better understanding of such flows than we currently have. These flows are poorly understood, not least because there are no field experiments that have followed the development of the turbulent wind and temperature fields over a hill of simple geometry under stable conditions. As a first attempt to do this without the enormous expense of a multi-tower field study we have performed a wind tunnel experiment where a heated model canopy on a low two-dimensional ridge was mounted upside down on the roof of the tunnel to generate a stable flow.

2. THE MODEL

Modelling diabatically unstable atmospheric boundary layers in wind tunnels requires very expensive facilities that allow a stable density gradient to be set up at the inlet to the working section. This stable gradient is necessary to limit the depth of the unstable layer produced by heating the floor. It is intrinsically easier to produce a stably stratified equilibrium boundary layer because the depth of stable layers is self limiting. In contrast to unstable layers, stable buoyancy forces oppose vertical diffusion of the layer. Turning the model upside down and mounting it on the wind tunnel roof reverses the influence of gravity and allows us to heat the model electrically rather than taking the technically more difficult path of cooling the floor.

The model canopy is made of bluff metal strips, 50mm high by 10mm wide. The heat flux from these canopy elements and from the model floor can be controlled independently. The geometry of the model is identical to the 'tombstone' canopy model studied by Raupach et al. (1986) and whose turbulence characteristics are well understood. The new surface will be referred to henceforth as Tombstones Heated or TH. The experiment was performed in the CSIRO PYE Laboratory Boundary Layer Wind Tunnel (WT). This facility is an open return circuit blower tunnel which has a working section (WS) 16m long, 1.8m wide with an adjustable roof. At the model position the mean roof height was ~0.75m but increased in the downwind direction to ensure $d\langle\bar{p}\rangle/dx = 0$, where x is the downwind coordinate and $\langle\bar{p}\rangle$ the mean static pressure (see comments on notation in section 2.2). Flow conditioning devices produced a thick equilibrium turbulent boundary layer at the start of the canopy model. The model surface consisted of a number of sections placed in the following windward sequence:

- (1) 5m of a very rough pebble surface
- (2) 2 m of the original unheated 'tombstone' model canopy surface
- (3) 1.05 m of the original 'tombstone' surface but with a heated floor.
- (4) 0.5 m of the new TH surface
- (5) A 50 mm high, ~1.1 m long sinusoidal hill covered with the new TH surface
- (6) A further 0.5m of the heated TH surface
- (7) A flat unheated rough surface 1.2 m long. (Pebble surface)

Hence the momentum boundary layer is allowed to adjust to the unheated tombstone surface before encountering the heated tombstones. The flux from the heated floor of the tombstone surface was 400w/m^2 . Over the new TH surface, this flux was split equally between 200w/m^2 from the floor and 200w/m^2 from the canopy elements.

*Corresponding author address: John Finnigan, CSIRO Marine and Atmospheric Research, GPO Box 3023, Canberra, ACT, 2601. Australia. e-mail: john.finnigan@csiro.au

2.1 Instrumentation

Two component streamwise, u and vertical, w velocities were measured with a TSI Laser Doppler Velocimeter mounted on a computer controlled 3D traverse gear. Mean and turbulent air temperatures were measured with a fine wire type T thermocouple with its junction located just outside the laser beam focus. Element and floor surface temperatures were measured with in situ thermistors and also with an Agema imaging infra red camera.

2.2 Notation

We use here the meteorological convention of a right handed coordinate system $\{x,y,z\}$ with x in the streamwise, z in the surface normal and y the transverse direction. Corresponding velocity components are $\{u,v,w\}$. Time averages are denoted by an overbar and fluctuations around the time mean by a prime, thus $u = \bar{u} + u'$. All turbulence statistics reported here are also averaged in the y direction for a distance $\pm 5h_c$ about the tunnel centreline where h_c is the canopy height of 50mm. This spatial averaging is denoted by $\langle \rangle$, thus, the turbulent shear stress is written as $\langle \overline{u'w'} \rangle$.

3. RESULTS

3.1 Froude Number and Reynolds Number Similarity

Dynamical similarity between real world and WT model flows relies on equality of the dimensional groups that describe key processes. The two groups that are critical here are the Reynolds Number (Re) and the Froude Number (Fr). Equality of Re ensures equality of the balance between inertial and viscous forces in the flow. The Reynolds Number is defined as,

$$Re = \frac{UL}{\nu} \quad (1)$$

where U and L are characteristic velocity and length scales of the flow, respectively and ν is the kinematic viscosity. Wind tunnel models cannot approach real world values of Re. In the atmosphere, Re is typically $O[10^8]$ whereas

in the WT, Re is $O[10^5-10^6]$ at best. Fortunately, if the flow is fully rough, that is, if most of the momentum transfer to the surface occurs through pressure forces on bluff surface elements rather than by viscous friction, we can achieve dynamical similarity of the main features of the flow at much lower Re.

Similarity of the Froude Number ensures equality of the balance of inertial and buoyancy forces on the flow.

$$Fr = \frac{NL}{U} \quad (2)$$

where N is the Brunt-Väisälä frequency defined as,

$$N = \frac{g}{T_0} \frac{\partial \theta}{\partial z} \quad (3)$$

with g the acceleration of gravity, T_0 a reference temperature, θ the potential temperature and z the vertical coordinate. Buoyancy forces become significant when $Fr < 1$.

It is clear that achieving similarity (or near similarity) of both Re and Fr imposes conflicting requirements on the modelling. Since L is set by model scale, we require U to be as large as possible for Re similarity but U to be as small as possible for Fr similarity. Since the only other variable within our control, the temperature gradient, $\partial \theta / \partial z$ is constrained by available power and fire regulations, we changed Fr by reducing U as far as possible while still maintaining realistic wind and turbulence profiles.

In Figure 1 we compare mean velocity and shear stress profiles at a series of stations upwind and over the model hill at a free stream velocity of $U_0 = 0.3 \text{ ms}^{-1}$, a velocity which allows us to attain $Fr < 1.0$, and at $U_0 = 10.0 \text{ ms}^{-1}$, which we know produces realistic turbulent statistics. It is clear that the high speed and low speed profiles are very similar for both statistics giving us some confidence that the gross dynamics of the natural gravity current will be represented properly in the WT model.

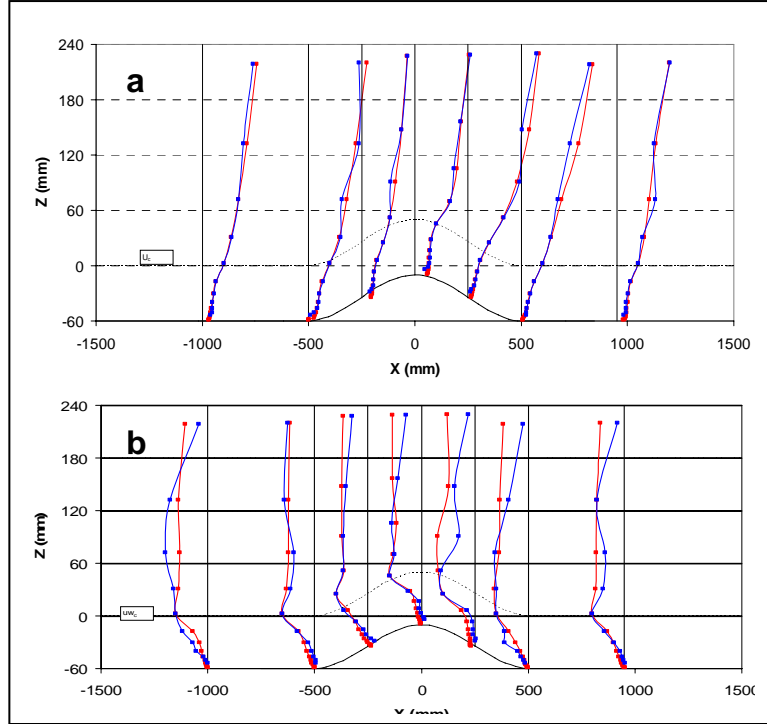


Figure 1. comparison of mean velocity $U(z) = \langle \bar{u} \rangle(z)$ and shear stress $\langle \overline{u'w'} \rangle$ profiles at free stream velocities of $U_0 = 10 \text{ ms}^{-1}$ (red) and $U_0 = 0.3 \text{ ms}^{-1}$ (blue). (a) $U(z)/U_0$. (b) $\langle \overline{u'w'} \rangle(z) / \langle \overline{u'w'} \rangle(h_c)$

3.2 Wind and Temperature fields: the gravity current

In Figure 2 we compare velocity profiles at a free stream wind speed of 0.3 ms^{-1} and with the model heating on and off. Profiles without heating (neutral stability) assume the characteristic form described and modelled by Finnigan and Belcher (2004) and Belcher et al. (2008). Well upstream of the hill, the velocity has a quasi-exponential shape within the canopy and a quasi-logarithmic shape in the boundary layer above with a distinct inflection point at the canopy top. Within the canopy, the maximum velocity speed-up occurs roughly half way up the windward slope of the hill while on the lee slope, just behind the crest, the velocity is strongly retarded near the ground. Finnigan and Belcher (2004) predicted that even on hills with very low slope like this model, if the canopy was sufficiently dense, flow reversal could occur in this region, a prediction that has since been confirmed in flume experiments (Poggi and Katul, 2007) and LES simulations (Prof. G. G. Katul and Dr E. G. Patton, pers. comm.). Above the canopy, the maximum speed up is over the hill crest as expected.

When the heat is turned on, which results in $Fr \sim 0.3$, the flow field changes fundamentally. Note that $Fr = U/NL$ is calculated with $L = L_h = 0.5$. L_h , the hill length scale, is conventionally taken as the distance from crest to half height point. We approximate the temperature gradient by a finite difference $\partial \langle \bar{\theta} \rangle / \partial z \approx \Delta \langle \bar{\theta} \rangle / \Delta z$ where Δz is the mean depth of the thermal layer over the hill ($\sim 300 \text{ mm}$ - see Figure 4) and $\Delta \langle \bar{\theta} \rangle$ the temperature change across it. First we see the appearance of a downslope gravity current on the windward side of the hill. This gravity current occupies the full canopy depth and extends to roughly $x = -10L_h$ on the flat surface upwind of the hill. Second we see that the wind speed within the canopy at the hill crest is practically zero except in the upper 20% of the canopy. Third we note that the downslope gravity current on the lee slope is less pronounced but that the tendency to reversed flow in the lee of the crest has disappeared.

In Figure 3 we plot the temperature profiles at the same x positions as in Figure 3. Note that the heated surface extends upwind only to $x = -2000 \text{ mm}$. Three features are noteworthy. First, with both floor and canopy elements

heated equally, the stable temperature gradient extends down to the surface through the canopy. This is typical of more open forest canopies at night whereas canopies with

closed crowns and open trunk spaces are usually stably stratified through the crown and unstable or neutral through the trunk space.

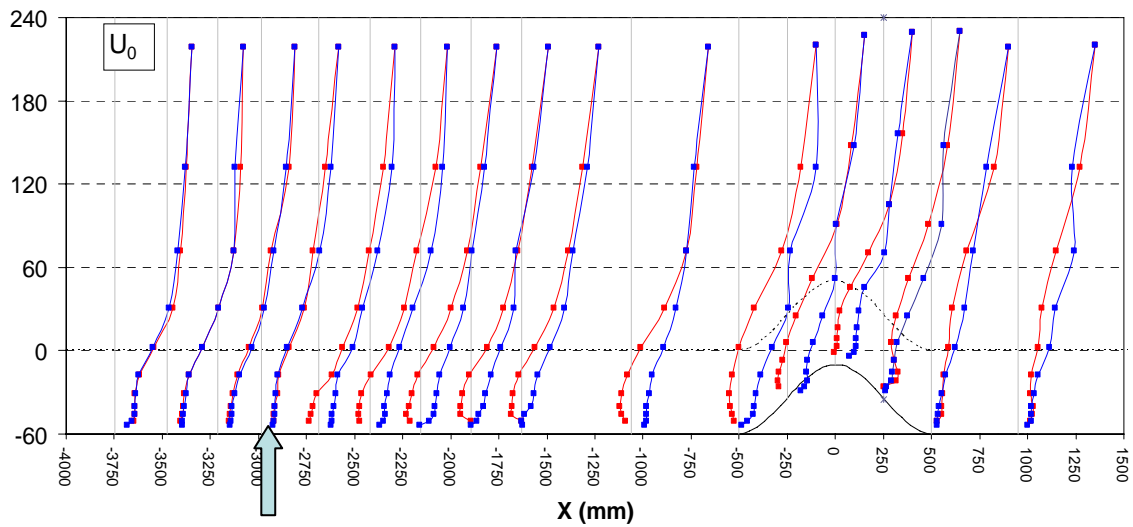


Figure 2. Comparison of mean velocity profiles plotted as $U(z)/U_0$ with the heating off (blue profiles) and the heating on (red profiles). The free stream velocity was $U_0 = 0.3ms^{-1}$. The broad arrow marks the upwind penetration of the gravity current.

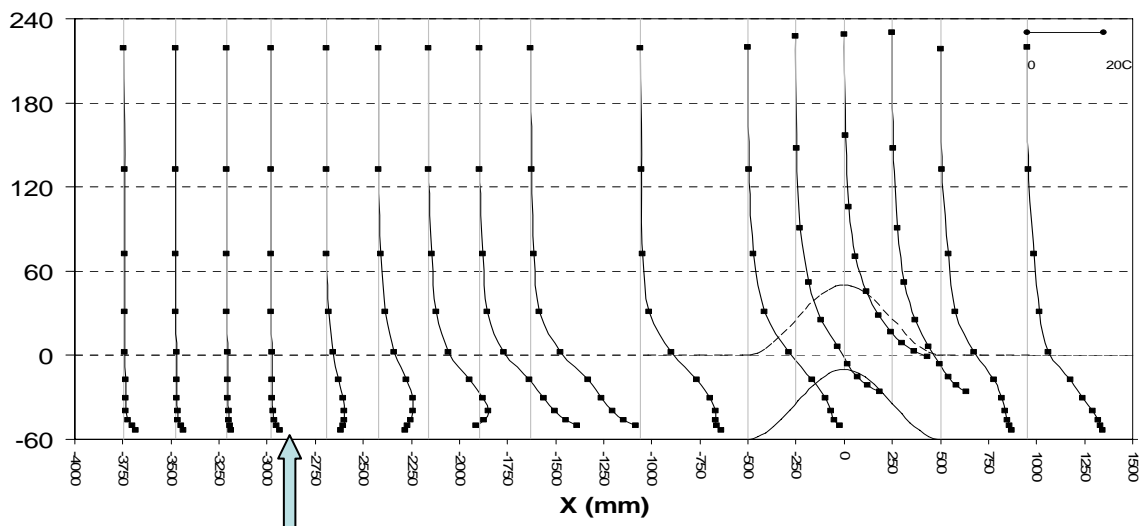


Figure 3. Profiles of the departure of local air temperature from the free stream temperature, T_0 . Temperature scale in degrees C is in top right.

Second, the magnitude and depth of the thermal internal boundary layer or gravity current reaches a maximum at the upwind foot of the hill. Third, the gravity current extends to $x=-3000$ mm, almost a metre upwind of the heated section of the floor.

4.0 Analysis

To understand the coherent nature of the gravity current and its remarkable upwind extent, it is necessary to analyze the balance of forces on the flow. We can do this by comparing the terms in the streamwise momentum balance, equation (4),

	hydrodynamic pressure gradient	hydrostatic pressure gradient	thermal wind	shear stress divergence	canopy drag
--	-----------------------------------	----------------------------------	-----------------	----------------------------	----------------

$$\frac{\partial \langle \bar{u} \rangle}{\partial t} + \langle \bar{u} \rangle \cdot \nabla \langle \bar{u} \rangle = -\frac{\partial \langle \bar{p} \rangle}{\partial x} + \frac{g}{T_0} \left(\Delta \langle \bar{\theta} \rangle \sin \alpha - \frac{\partial (\Delta \hat{\theta} h)}{\partial x} \cos \alpha \right) - \frac{\partial \langle \bar{u}'w' \rangle}{\partial z} - C_d a |\langle \bar{u} \rangle| \langle \bar{u} \rangle$$

(4)

The two terms on the left hand side of the equation comprise the total flow acceleration while on the right hand side we have first the hydrodynamic pressure gradient, $\partial \langle \bar{p} \rangle / \partial x$, which results from the deflection of the wind around the hill. The next two terms in blue are the contributions of the gravity current to the total pressure gradient. The first, the hydrostatic pressure gradient is the downslope resultant of the gravity force on air parcels with temperature deficit $\Delta \langle \bar{\theta} \rangle$. The second term, the thermal wind term, is present if there is a slope in the depth of the gravity current as this means that the pressure generated at any level by the density anomaly above, changes in the x direction. This is the process that, at a much larger scale, drives the sea breeze. The next term is the shear stress divergence while the last is the aerodynamic drag of the canopy, which always opposes the flow direction. The angle of departure of the streamline from the horizontal is denoted by α and $\Delta \hat{\theta}$ is the temperature deficit averaged from height z to the top of the gravity current, which is at height h. For a full derivation of this equation, see Mahrt (1982).

A series of processes occurs when real canopies cool radiatively at night. The first and most critical is that as the flow above the canopy becomes weakly stable, the flow within the canopy becomes strongly stable with gradient Richardson numbers, $Ri = N^2 / (\partial U / \partial z)$ rapidly becoming $O[10]$ and leading to a collapse of turbulent mixing. The reason for this lies ultimately in the different mechanisms of transport of heat and momentum to the foliage, which ensure that the windspeed approaches its leaf surface value of zero much more rapidly than the air temperature approaches the leaf temperature. As a result, while the velocity gradient rapidly goes to zero in the upper canopy, the temperature gradient continues down to the surface. As can be seen from the form of Ri, this leads to large values of Ri as $\partial U / \partial z$

becomes small (Belcher et al, 2008). When $Ri > 0.25$, vertical turbulent mixing is strongly suppressed.

In our WT model, we see the same phenomenon and shear stress, $\langle \bar{u}'w' \rangle$ collapses within the canopy when the heat is on and the flow stably stratified. Our WT flow was steady state so the temporal acceleration can be ignored while the spatial acceleration terms, $\langle \bar{u} \rangle \cdot \nabla \langle \bar{u} \rangle$ could not, of themselves, produce a reversal in flow direction. This meant that the resultant flow direction within the canopy was set by the balance of the three pressure gradient terms as the aerodynamic drag can only oppose the resultant flow. The hydrodynamic pressure gradient accelerates flow over the hill and cannot produce a downslope flow on the upwind face of the hill. In fact as we see from Figure 3, it opposes the gravity current. The effect of the hydrostatic pressure gradient is confined to the hill slope or as far upwind and downwind as the streamlines are not parallel to the geopotential. Hence the only term capable of driving the gravity current against the advecting mean flow and hydrodynamic pressure gradient is the thermal wind term.

In Figure 4 we plot the shape of the thermal boundary layer in terms of its height averaged temperature anomaly $\langle \theta \rangle$ and its temperature displacement height, h^* ,

$$\langle \theta \rangle = \frac{1}{h} \int_0^h \langle \bar{\theta} \rangle(z) dz \quad (5)$$

$$h^* = \int_0^h \frac{\langle \bar{\theta} \rangle(z) - \langle \bar{\theta} \rangle(0)}{\langle \bar{\theta} \rangle(0)} dz \quad (6)$$

h is the depth of the thermal layer and h^* is the depth the thermal layer would have if it had a constant temperature $\langle \theta \rangle$. We see that both

the displacement height and the average temperature anomaly peak around the upwind foot of the hill. The depth of the temperature anomaly then decreases downwind but more steeply upwind. The definition of the thermal

wind term in equation (4) shows that this term, will tend to drive flow upwind to the left of its peak at the foot of the hill and downwind to the right of its peak.

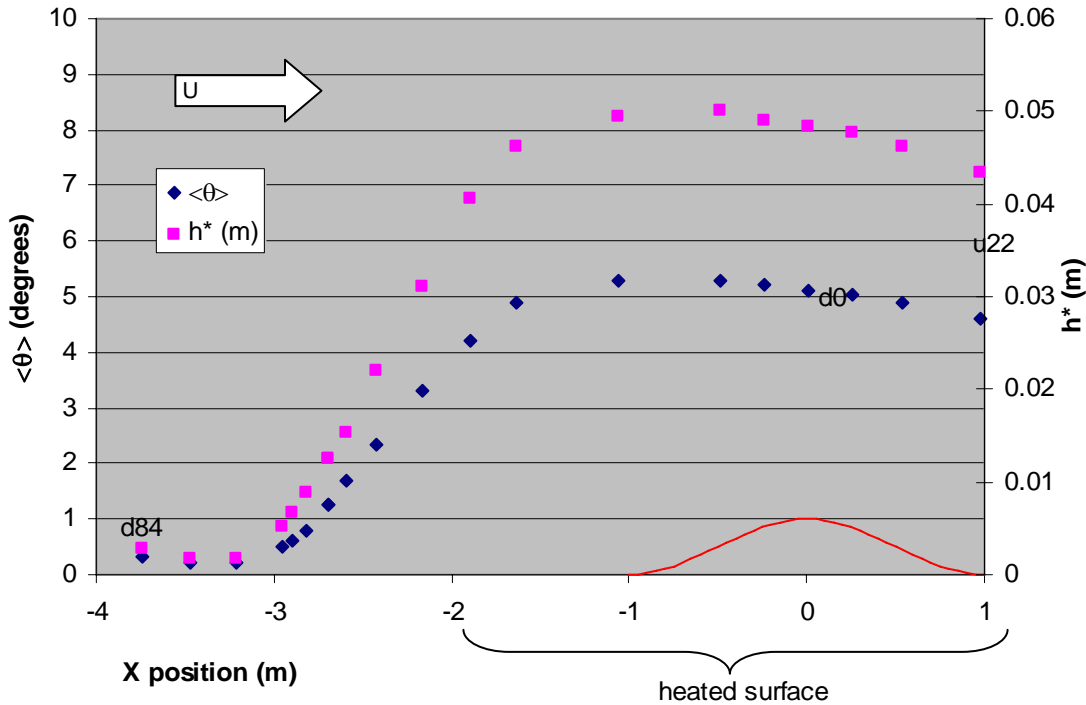


Figure 4. The average temperature deficit of the gravity current $\langle \theta \rangle$ and the displacement height of temperature, h^* . The temperature scale is on the left axis in deg C.

In Figure 5 we have compared the thermal wind, the hydrostatic and the hydrodynamic pressure terms calculated at the surface. Note that the hydrodynamic and hydrostatic terms are approximations. The former was calculated assuming inviscid flow over the sinusoidal hill as we did not make direct

measurements of surface pressure, while the hydrostatic term was calculated using the surface slope and the averaged temperature anomaly $\langle \theta \rangle$. Hence this latter term should be viewed as a lower bound.

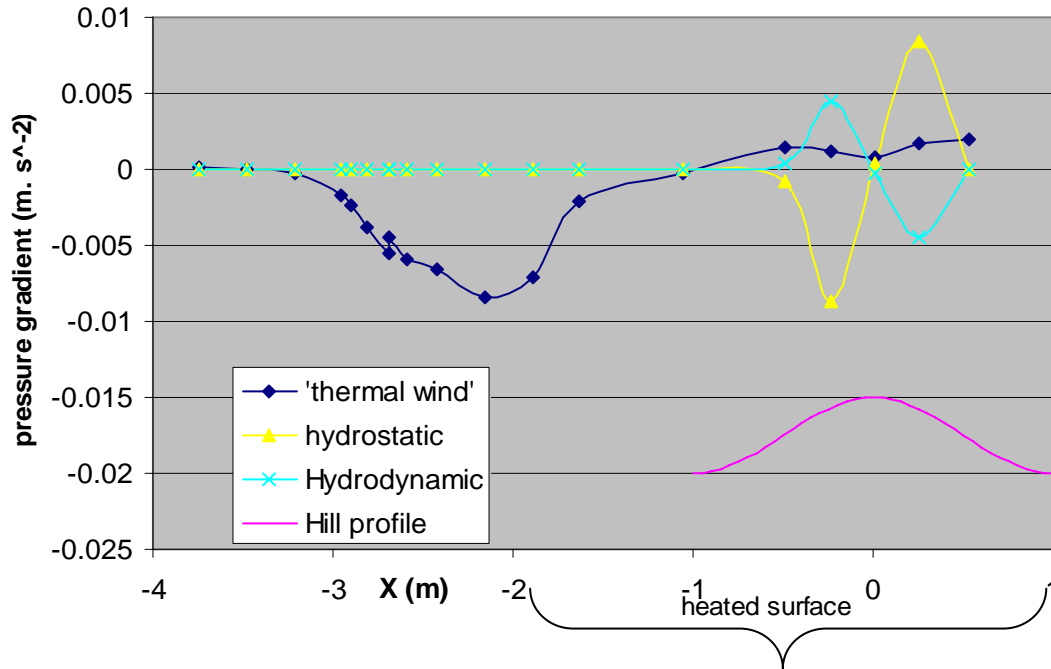


Figure 5. Comparison of the hydrostatic, hydrodynamic and thermal wind terms calculated at the hill surface. Note that the hydrodynamic term was calculated by assuming inviscid flow as surface pressure was not measured in this experiment. Similarly, the hydrostatic pressure gradient was calculated using the surface slope and the averaged temperature anomaly $\langle \theta \rangle$.

We see that on the hill itself, the hydrodynamic and hydrostatic terms are in opposition with the hydrostatic term tending to drive flow downslope on both sides of the crest while the hydrodynamic pressure does the opposite. In contrast, the thermal wind term is relatively small over the hill, peaking well upwind where the slope of the gravity current is largest. It is clear that it is this term that is responsible for driving the within-canopy gravity current so far upwind of the hill onto the flat surface. As the gravity current penetrates upwind of the heated surface, it carries heat with it to maintain the density anomaly that drives it. Although not shown here we also note that at the termination of the gravity current, heat transfer from the canopy to the boundary layer above, increases suddenly to almost 5 times its downwind value.

4. DISCUSSION AND CONCLUSIONS

We have constructed a WT model of stably stratified flow over a low hill covered with a tall plant canopy such as a forest. Dynamical similarity was achieved at flow speeds that allowed us to attain Froude numbers less than one. For $Fr < 0.5$ we saw the establishment of a thick stable gravity current that was promoted by the collapse of turbulent mixing in the canopy. This phenomenon is widely observed in the field after sunset and is a result ultimately of the

differing mechanisms of heat and momentum transfer across the foliage or canopy element surfaces (Belcher et al. 2008). Much to our surprise, the gravity current not only reversed the flow direction within the canopy on both sides of the hill but penetrated far upwind of the hill on the flat surface. At the terminus of the current, we observed a spike in heat transfer from the canopy.

As gravity currents such as these are implicated in the failure to measure respiration fluxes at tower sites on stable nights we were concerned to understand the dynamics of this phenomenon. After turbulence has collapsed, downslope and counter-flow gravity currents can occur if the hydrostatic pressure gradient exceeds the hydrodynamic gradient on the hill. On a low hill, the hydrodynamic gradient can be shown to be of order,

$$\frac{\partial P}{\partial x} \sim \frac{H}{L_h^2} U_0^2 \quad (7)$$

where H is hill height and L_h the distance from crest to half height point (Finnigan and Belcher, 2004). The hydrostatic gradient can be scaled similarly as,

$$g \frac{\Delta\theta}{T_0} \frac{H}{L_h} \quad (8)$$

The ratio of these two pressure gradients has the form of the square of a Froude No,

$$Fr^2 = -\frac{H}{L_h^2} U_0^2 \Big/ g \frac{\Delta\theta}{\Theta_0} \frac{H}{L_h} \rightarrow Fr = \sqrt{-\frac{U_0^2}{gL_h} \frac{\Theta_0}{\Delta\theta}} \quad (9)$$

Surprisingly, the ratio of these two quantities, whose value controls the onset of the downslope flow, does not contain the slope of the hill, H/L_h but only the hill length, L_h , the temperature anomaly $\Delta\theta$ and the windspeed squared, U_0^2 . This could explain why advective gravity currents are often seen at night at sites which have only very gentle slopes and where advection is not a problem by day.

In order to explain the penetration of the gravity current far upwind of the hill, we had to consider the thermal wind term, which, on scaling grounds, is usually ignored in these situations. It is this term which provides the necessary upwind forcing. Two factors produce the slope of the temperature anomaly and the resulting thermal wind pressure gradient. The first is the conflict between the downslope advection of heat within the canopy on the upwind side of the hill and the advection of heat from upwind. This results in the maximum thickness of the thermal anomaly being above the upwind foot of the hill. The second is the finite extent of heated surface in our model, which ensures a significant slope in the depth of the thermal anomaly upwind of the hill. If the former effect is dominant we can expect to see this on any isolated hill with consequences for the siting of flux towers. If it is the latter, then it should disappear when we repeat the experiment with a much longer extent of heated surface. We are currently planning to repeat the experiment with at least double the length of heated canopy to answer this question.

5. REFERENCES

Baldocchi, D.D., Falge, E., Gu, L., Olson, R., Hollinger, D., Running, S., Anthoni, P., Bernhofer, Ch., Davis, K., Evans, R., Fuentes, J., Goldstein, A., Katul, G., Law, B., Lee, X., Malhi, Y., Meyers, T., Munger, W., Oechal, W., Paw U, K.T., Pilegaard, K., Schmid, H.P., Valentini, R., Verma, S., Vesala, T., Wilson, K., Wofsy, S., 2001: FLUXNET: A new tool to study the temporal and spatial variability of ecosystem-scale carbon dioxide, water vapour and

energy flux densities. *Bull. Amer. Meteorol. Soc.* 82; 2415-2434

Belcher, S. E., J. J. Finnigan and Harman, I.N., (2007.: Flows through forest canopies in complex terrain, *Ecological Applications* (In Press)

Finnigan, J.J. and Belcher, S.E., 2004: Flow over a hill covered with a plant canopy. *Quart. J. Roy. Meteorol. Soc.* 130, 1-29

Mahrt, L. 1982: The Momentum balance of Gravity Flows. *J. Atmos. Sci.* 39, 2701–2711

Poggi, D., and G.G. Katul, 2007: Turbulent flows inside forested hilly terrain: the recirculation region, *Quarterly Journal of the Royal Meteorological Society*, 133, 1027-1039

Raupach, M.R., Coppin, P.A., Legg, B.J., 1986: Experiments on Scalar Dispersion Within a Model Plant Canopy. Part I: The Turbulence Structure, *Boundary-Layer Meteorol.* 35, 21-52.

Staebler, R.M. and Fitzjarrald, D.R., 2005: Measuring canopy structure and the kinematics of subcanopy flow in two forests. *J. Appl. Meteorol.* 44, 1161-1179